Mid-IR plasmonic compound with gallium oxide toplayer formed by GaSb oxidation in water

Mario Bomers, Davide Maria Di Paola, Laurent Cerutti, Thierry Michel, Richard Arinero, Eric Tournié, Amalia Patanè, Thierry Taliercio

Mid-IR plasmonic compound with gallium oxide toplayer formed by GaSb oxidation in water

Mario Bomers,[1,*] Davide Maria Di Paola,[2] Laurent Cerutti,[1] Thierry Michel,[3] Richard Arinero,[1] Eric Tournié,[1] Amalia Patanè,[2] and Thierry Taliercio[1]

1 IES, Université de Montpellier, CNRS, Montpellier, France
2 School of Physics and Astronomy, The University of Nottingham, Nottingham NG7 2RD, UK
3 L2C, Université de Montpellier, CNRS, Montpellier, France

Abstract: The oxidation of GaSb in aqueous environments has gained interest by the advent of plasmonic antimonide-based compound semiconductors for molecular sensing applications. This work focuses on quantifying the GaSb-water reaction kinetics by studying a model compound system consisting of a 50 nm thick GaSb layer on a 1000 nm thick highly Si-doped epitaxial grown InAsSb layer. Tracing of phonon modes by Raman spectroscopy over 14 h of reaction time shows that within 4 hours, the 50 nm of GaSb, opaque for visible light, transforms to a transparent material. Energy-dispersive X-ray spectroscopy shows that the reaction leads to antimony depletion and oxygen incorporation. The final product is a gallium oxide. The good conductivity of the highly Si-doped InAsSb and the absence of conduction states through the oxide are demonstrated by tunneling atomic force microscopy. Measuring the reflectivity of the compound layer structure from 0.3 µm to 20 µm and fitting of the data by the transfer-matrix method allows us to determine a refractive index value of 1.6 ± 0.1 for the gallium oxide formed in water. The investigated model system demonstrates that corrosion, i.e. antimony depletion and oxygen incorporation, transforms the narrow band gap material GaSb into a gallium oxide transparent in the range from 0.3 to 20 µm.

1. Introduction

Antimonide-based compound semiconductors are promising narrow band gap materials for fast and low power consuming electronics [1], for mid-IR opto-electronic applications [2], for waveguide and optical parametric oscillator fabrication [3,4], for photovoltaics [5–7] and for plasmonic applications [8,9]. Developing a more comprehensive understanding of GaSb-compounds in aqueous environments is particularly important for biosensing applications in the mid-infrared spectral range [10]. Actually, the slow, steady and selective oxidation of GaSb in water leads to an all-semiconductor mid-IR pedestal configuration consisting of highly doped InAsSb plasmonic resonators on top of GaSb pedestals embedded in an amorphous oxide layer [11]. During the GaSb oxidation in water the group V-element Sb is depleted. A similar preferential dissolution of the group V-element was reported for the III-V semiconductor GaAs in aqueous environments [12].

On the one hand, there is an interest in better understanding of the hydrolytic instability of GaSb; on the other hand the galliums oxide formed by the reaction in water is of interest as it can serve for divers applications, e.g. the preparation of gas sensors, catalysts, phosphors, and optoelectronic devices [13–15]. The gallium oxide (Ga_2O_3), known as gallia, is an important semiconductor with a wide band gap of 4.9 eV, which can serve as a high-conductivity material for transparent electrodes. Synthesis in aqueous solution leads to polymorph gallia [14], but the homoepitaxial growth by metal organic vapor phase epitaxy leads to single-phase thin films of $\beta - Ga_2O_3$, whichs can be Si-doped [16].

The literature on GaSb oxidation distinguishes between the few nanometer thin native GaSb oxide formed in air and the much thicker oxide layers formed by plasma-, temperature- or wet-chemical oxidation. The native GaSb oxide is due to a thermodynamic equilibrium of GaSb and air, which leads to the formation of Ga_2O_3 and Sb_2O_3 [17,18]. In a long-time oxidation study, the stability of the thin native oxide layer (< 4 nm) was demonstrated [19]. However, the further oxidation of GaSb and Sb_2O_3 gives rise to elemental Sb, which is responsible for high surface leakage current [20]. Sulfur passivation can reduce the surface leakage current [20] and improve device performance [21–23], but the prevention of surface re-oxidation might only last a short-time (< 1 day) [24].

Further insight in the oxidation reaction mechanism at the semiconductor/oxygen interface was recently obtained by scanning tunneling microscopy measurements which exploited the controlled exposure of a clean GaSb surface to oxygen [25]. The research on the reaction mechanism at GaSb/solution interfaces is ongoing and a recent study has shown that the redox processes are relevant for modifying the surface's electronic structure of GaSb during the reaction with an aqueous sodium sulfide solution [26]. In the field of plasmonic applications, a recent work has also demonstrated that the native oxide of GaSb can be exploited for stable surface functionalization based on phosphonic acid chemistry [27].

Top-down technological processes depend on controlled and selective etching of antimonide-based compound semiconductors [28,29]. As etching consists of oxidation and reduction, two recent studies investigate the role of H_2O_2 and H_2O as oxidizers for GaSb etching [30,31]. Contrary to InAs and $InAs_{0.9}Sb_{0.1}$ which are chemically stable in water [32], GaSb oxidizes in aqueous environment. The GaSb oxide formed by immersion of GaSb for two hours in water contains still significant quantity of Sb_2O_3 which is thermally unstable and can lead to unwanted conduction channels [33]. The electro-chemical process of anodic oxidation accelerates the process of GaSb oxidation. Therefore oxide layers, several hundreds of nanometer thick, can be formed in few minutes [34]. Compared to anodic oxidation, the GaSb oxidation in water is not driven by an external electro-chemical potential, but by exothermic reactions of GaSb with water, as demonstrated by density functional theory [35]. Antimony oxides are soluble in water [36] and therefore lead to corrosion. Gallium oxides are non-soluble in pure water [37].

In this work, we study a model compound system consisting of a 50 nm thick GaSb layer epitaxially grown on a 1000 nm thick layer of highly Si-doped InAsSb. The reaction of the GaSb with water over a period of 14 h is investigated by Raman spectroscopy, energy-dispersive X-ray spectroscopy, conductive atomic force microscopy and reflectometry in the visible and infrared spectral range. Electro-optical parameters of GaSb and InAsSb, [38,39], spectral ellipsometrically determined constants of GaSb [40] and its anodically grown oxide [41,42], as well as the electro-optical constants of gallium oxides [43–45] and of antimony oxide [46,47] allow us to assess the product of the GaSb oxidation in water. In particular, we report a refractive index of $n = 1.6 \pm 0.1$ for the oxide, which is closer to the reported value of n=1.68 for GaO_x [44] than the value reported for anodically grown GaSb oxide (n=2.0).

2. Materials and Methods

Solid-source molecular beam epitaxy (MBE) was used to grow 50 nm of GaSb on top of a 1000 nm thick Si-doped $InAs_{0.9}Sb_{0.1}$ layer. These two layers were grown on top of a 300 nm non-doped GaSb buffer layer, after the commercial available Te-doped (001) GaSb substrate was thermally de-oxidized under high vacuum conditions in the MBE-chamber. A doping level of $5x10^{19}$ cm^{-3} was determined for the $InAs_{0.9}Sb_{0.1}$ layer [48]. The highly-doped $InAs_{0.9}Sb_{0.1}$-layer acts as a stop layer for the chemical reaction of the GaSb toplayer in water and as a mid-IR mirror for wavelength above the plasma wavelength, which is 5.5 µm for this doping level. The grown wafer was cleaved into 8 smaller pieces and each sample was immersed for a different amount of time in beakers filled with distilled water purified by the Purelab Option-Q and with resistivity of 13.4 MΩ·cm at 23°C. After a specific reaction time, the samples were removed and blown dry by nitrogen gas. For characterizing the samples, micro-Raman spectroscopy (Renishaw inVia microscope) was performed with an x50 objective, 532 nm excitation laser wavelength, 3.4 mW incident power and 1 s acquisition time. Raman peaks were fitted with Lorentzians using the Fityk software [49]. Scanning electron microscopy (Fei Inspect S-50) was used to trace changes in the chemical composition by working in the energy-dispersive X-ray spectroscopy mode with an incident electron-beam energy of 8.0 kV and a magnification of x5000. Information on the surface topography and conductivity were obtained by tunneling atomic force microscopy (TUNA) with the NanoMan AFM (Bruker) equipped with a metal coated tip (PPP-ContPt-50). The reflectivity of the sample was measured in the visible spectral range by the Sopra GES-5 ellipsometer for an incident angle of 60° and an aluminum mirror as reference to normalize the reflectivity. In the IR-spectral range the Vertex 70 Fourier-transform IR (FTIR) spectrometer (Bruker) was used to measure the reflectivity of the samples for an incident angle of 60° and with a gold mirror as reference to normalize the spectra.

3. Raman spectroscopy to trace material transition of GaSb in water

The MBE grown layer structure, subdivided into smaller samples and immersed for different time duration in water filled beakers, was investigated by Raman spectroscopy after drying by inert lab gas and storage at ambient conditions. In Figure 1, the results of the Raman spectroscopy measurements are shown. The spectral region with significant phonon modes is shown in (a) and the spectral range with a plasmonic mode and fluorescence is shown in (b). The spectra were vertically shifted to clarify the identification of spectral features. In particular, in Figure 1(a) clear changes of the active phonon modes can be seen. For the samples not immersed in water (0 h) or immersed for less than 4 h in water, the most dominant Raman shift are observable at 236 cm^{-1} and at 227 cm^{-1}. These peaks nearly disappear in between 6 h to 8 h of immersion and additional peaks appear. After 6 h of reaction with water, spectral signatures at 140 cm^{-1} and at 217 cm^{-1} can be identified. In Figure 1(b), a spectral signature at 1783 cm^{-1} appears after 4 h of reaction with water. A broad signature, centered around 1100 cm^{-1}, can be observed after 6 h, then most strongly after 8 h, but finally it vanishes again after 14 h. We attribute this broad signature to fluorescence originating from Sb-oxide states [47]. The photon energy of the fluorescence is near 2.2 eV.

A literature comparison allows to assign the measured Raman peaks to phonon modes of binary constituents of the layer structure (see Table 1). The phonon peaks that are decreasing with reaction time are attributed to GaSb and those appearing with reaction time to InAsSb. The signature at 140 cm^{-1} is attributed to a disorder-activated

longitudinal acoustic (DALA) phonon of the InAsSb-layer [39]. The peak at 1783 cm^{-1} is attributed to a phonon–plasmon coupled mode Ω_+ where the plasmon is due to the Si-doping of the InAsSb layer [50]. In the limit of wavevector k ≈ 0, the frequencies for the phonon–plasmon modes are given by [51]

$$\Omega_{\pm}^2 = \frac{1}{2}\left[\left(\omega_p^2 + \omega_{LO}^2\right) \pm \sqrt{\left(\omega_p^2 + \omega_{LO}^2\right)^2 - 4\omega_p^2\omega_{TO}^2}\right] \quad , (1)$$

where ω_p is the plasma frequency, ω_{LO} the LO phonon frequency and ω_{TO} the TO phonon frequency of the InAsSb-layer. As $\omega_p \gg (\omega_{LO}, \omega_{TO})$ we find that $\Omega_- \approx \omega_{TO}$ and $\Omega_+ \approx \omega_p$ .The found value of $\Omega_+ \approx \omega_p = 1783\ cm^{-1}$ is in good agreement with the value of $\omega_p = 1818\ cm^{-1}$ obtained by the Brewster angle method used to determine the plasma wavelength of the wafer [48].

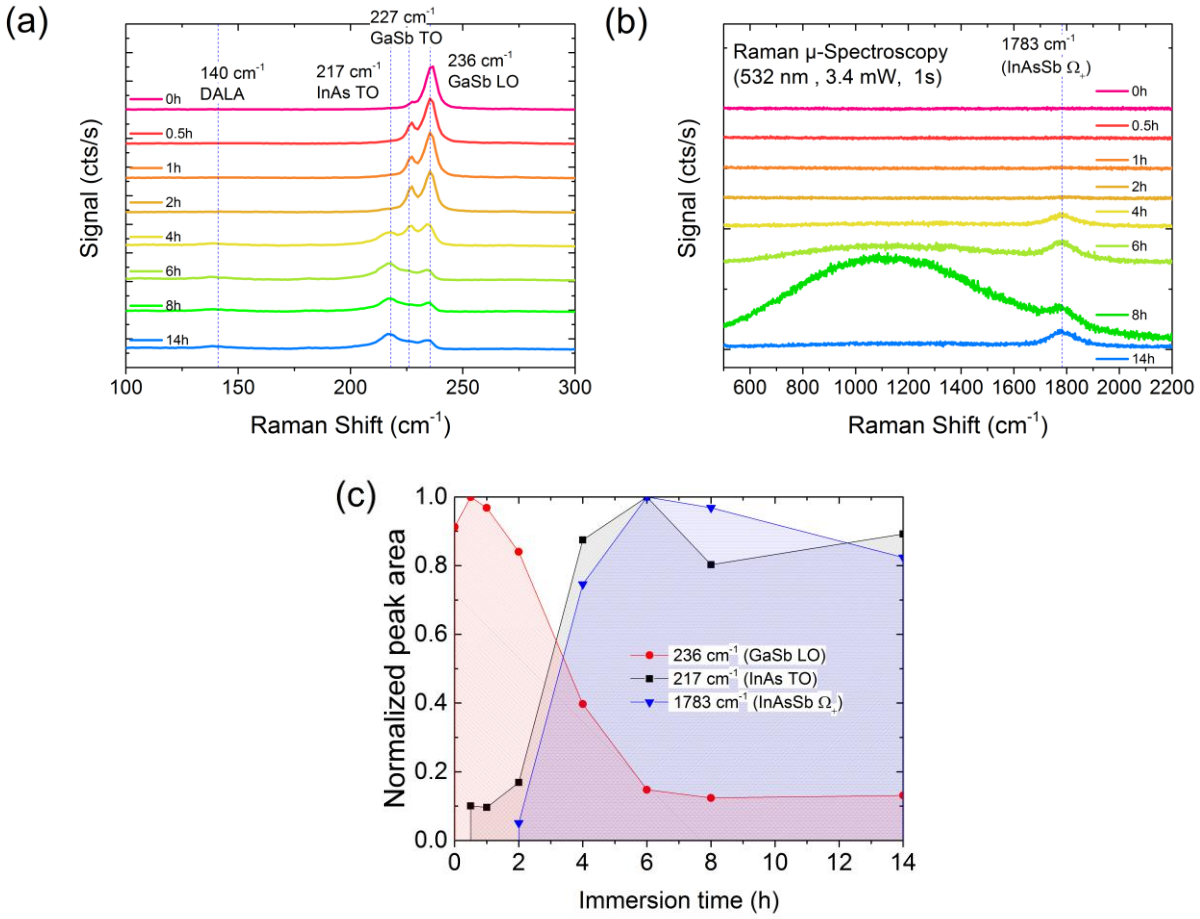

Figure 1: Raman spectroscopy performed with 532 nm excitation laser wavelength. (a) Measured phonon modes for GaSb / $InAs_{0.9}Sb_{0.1}$ compound system immersed for different amount of time to water (from 0 h to 14 h). (b) Measured fluorescence and plasmon mode of the compound system. (c) Normalized peak area versus reaction time (immersion time) in water.

Table 1: Phonon frequencies of binary constituents of the layer structure and the plasmon frequencies of the highly Si-doped InAsSb.

Compound	Mode	Shift (cm^{-1})	Mode	Shift (cm^{-1})
InAs [39]	TO	217.3	LO	238.8
GaSb [39]	TO	227.0	LO	236.0
InAsSb:Si	Ω_-	217.0	Ω_+	1783.0

The peak area for the signatures at Raman shifts of 236 cm^{-1}, at 217 cm^{-1} and at 1783 cm^{-1} were determined for all eight samples. In Figure 1(c), the evolution of the normalized peak area ratio is plotted versus the immersion time in water. It can be seen that the peak intensities attributed to GaSb decrease with immersion time and the modes attributed to InAsSb:Si increase with time. The intensity increase of the InAsSb modes is correlated with the disappearance of the GaSb modes. The immersion in water seems to transform the crystalline GaSb which absorbs strongly visible light (band gap at 0.72 eV) into a material transparent at 532 nm, thus the InAsSb:Si modes are no longer shielded by the 50 nm GaSb toplayer. After 6 hours the GaSb peaks reaches a plateau, which indicates that the material transformation is complete and the material is no longer crystalline GaSb, but composed of antimony and gallium oxides.

4. SEM and EDS measurements

Changes in the chemical composition of the 50 nm GaSb-toplayer were investigated by energy-dispersive X-ray spectroscopy (EDS). Three samples, immersed for different time duration in water, were chosen for the investigation. Additionally, a reference sample consisting of 1 µm InAsSb:Si without 50 nm toplayer was characterized.

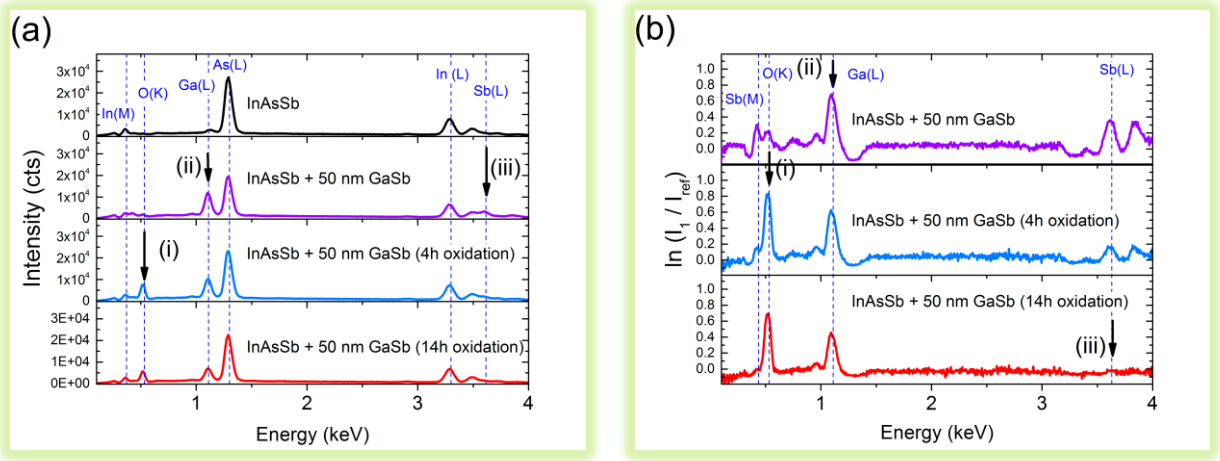

Figure 2: (a) Energy-dispersive X-ray spectra (EDS) of an InAsSb-layer without GaSb toplayer and of the compound system with GaSb toplayer are shown. The samples with toplayer were immersed for different time duration in water. (b) The spectra of the samples with toplayer are normalized to the reference spectra of an InAsSb-layer without toplayer to reveal changes in composition. The natural logarithm was taken to increase the contrast.

In Figure 2(a) the measured EDS spectra are shown. The spectrum of the reference sample, consisting of 1 µm of InAsSb:Si epitaxially grown on GaSb, is shown on top. Below, the spectra of the samples with GaSb toplayer and with different time of immersion in water are shown (without immersion, 4 h of immersion and 14 h of immersion). Changes in chemical composition are indicated by black arrows. To focus on changes in chemical composition of the 50 nm thin toplayer, the spectra of the samples with 50 nm thick toplayer were normalized to the InAsSb:Si reference spectra without GaSb toplayer. Furthermore, the natural logarithm of this ratio was taken to increase the contrast. The result of the data treatment is shown in Figure 2(b). The microscopes XPS-database allows to attribute the peaks to core-electron transitions. The spectral signature at 0.52 keV (i) can be assigned to the O(K) transition. Energetically close is the Sb(M) transition at 0.43 keV. Higher in energy are the Ga(L) line at 1.1 keV (ii) and the Sb(L) transition at 3.6 keV (iii). As the data treatment is optimized to reveal changes originating from the 50 nm toplayer, we clearly see in Figure 2(a) that the main elements found for the GaSb toplayer not immersed in water are antimony and gallium with a small amount of oxygen. Immersion to water leads to a strong decrease of the antimony peaks and a strong increase of the oxygen peak. While after 4 h of reaction, some residues of Sb are part of the toplayer, these residues have vanished after 14 h. The observed changes in chemical composition are in good agreement with the Raman results concerning the hypothesis of fluorescence originating from Sb-oxides, which vanish after 14 h of reaction time.

We conclude that the immersion of the 50 nm GaSb toplayer in water has two major consequences in terms of modifying the material: (1) an incorporation of oxygen and (2) a depletion of antimony, which can be controlled by the time of immersion in water.

Tunneling atomic force microscopy (TUNA)

To further investigate the topological and electrical properties of the gallium oxide layer, we applied tunneling atomic force microscopy (TUNA) to the sample immersed for 14 h in water. By exposing half of the oxidized sample for 10 s to HCl:H_2O (1:5), the oxide in contact with the etching solution was removed and the underlying InAsSb:Si was uncovered. The other half of the surface, not exposed to the acidic solution, was unchanged. The uncovered InAsSb:Si surface was then contacted by a gold clamp and atomic force microscopy measurements were conducted at the interface between the etched and the non-etched region. Figure 3(a) shows the topography and the thickness of the oxide film measured at this interface. We determine a thickness of 55 nm ± 5 nm. Thus we conclude that the oxidation process does not significantly modify the thickness of the former crystalline 50 nm thick GaSb toplayer. By positioning the conductive tip either on the oxide or on the InAsSb-surface, we could measure the electric current versus the applied voltage by the electric circuit formed by the gold clamp, the InAsSb-surface and the tip. For the sake of illustration a sketch is added to the inset of Figure 3(b). To obtain a reference current-voltage I-V curve, we used a gold surface with the same clamp system and the same tip. To obtain the highest current variation, the AFM tip was brought to contact with the surface such that ideally an ohmic contact is formed. The electronics of the TUNA microscope require to specify the detection range for low-current measurements. For the gold and the InAsSb-surface, a measurement range from -1.1 µA to 1.1 µA with current saturation outside of this range was chosen. On top of Figure 3(b), I-V characteristics for the gold reference sample are plotted. The current increases linearly with voltage, thus a typical ohmic behavior can be observed. On the bottom of Fig. 3(b), the I-V results with the same tip and clamping system, but on the InAsSb-surface are represented. Subsequently, we measured again the gold surface to check for tip degradation and we repeated the experiment with a second tip. We find that the gold reference system has about seven times higher conductivity than the highly Si-doped InAsSb layer. We explain the lower conductivity of the Si-doped InAsSb layer by the native oxide of the InAsSb surface, which increases the tunneling distance by 1-3 nm, and by the 1000 times higher charge carrier density in gold.

Finally, we measured the current when the tip was positioned on the oxide and the clamp on the InAsSb:Si surface. A flat I-V curve was measured, i.e. no tunneling current was measured through the oxide layer. We repeated the experiment in the measurement range from -1.1 nA to 1.1 nA, but no current could be measured. This results demonstrates that the gallium oxide formed by immersion of non-doped GaSb in water is electrically insulating.

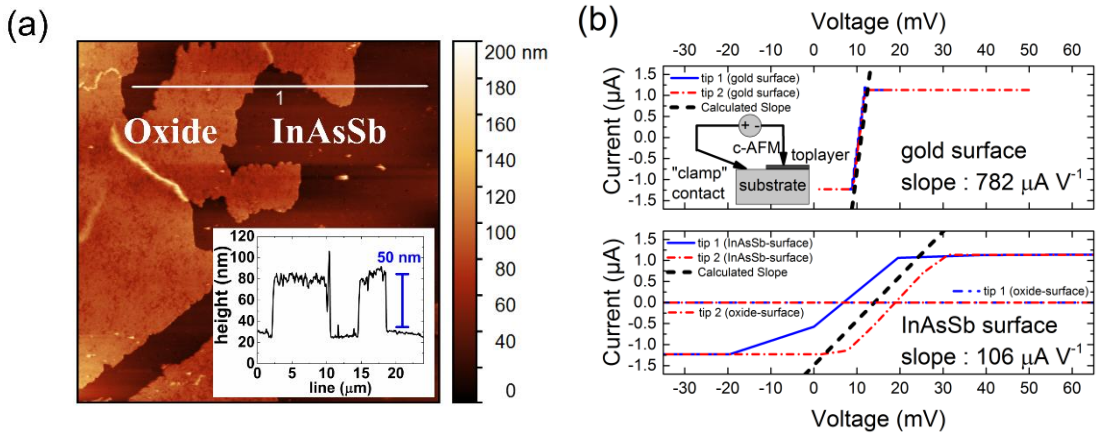

Figure 3: (a) Atomic force microscopy of the interface of the oxide and uncovered InAsSb surface. Inset: height profile acquired along line 1 in the main Figure. (b) Tunneling atomic force microscopy (TUNA) on the gold reference sample and on the GaSb / InAsSb compound structure. Inset: sketch of the electric circuit formed by clamp contact and AFM-tip.

5. Reflectometry and fitting by transfer-matrix method

Our structure and the controlled thickness of the oxide layer are very suited for a reflectometry experiment with subsequent fitting by the transfer-matrix method to determine the optical properties of the Ga-oxide formed in water. To cover a wide spectral range, the VIS- and the IR-spectral ranges were measured with two different experimental setups (reflectivity normalized by an Al-mirror in the VIS-range and by a gold-mirror in the IR-range). The result of

this reflection measurement is shown in Figure 4(a) for s- and for p-polarized light with an incident angle of 60 degrees. It can be seen that the reflectance properties change with increasing immersion time. The strongest modification is observed for ultraviolet light from 300-400 nm for s-polarized light; a dip in reflection is observed after the sample was exposed for more than 4 hours to water. In the IR-range, the modifications due to water immersion are perceptible as a shift of interference fringes. The onset of the highly reflective behavior is the plasma edge at 5.5 µm. While the Brewster mode [48], which is excited by p-polarized light, is nearly unaffected by the immersion process, the shift of a distinct dip in reflection is observed for s-polarized light in close proximity to the plasma edge.

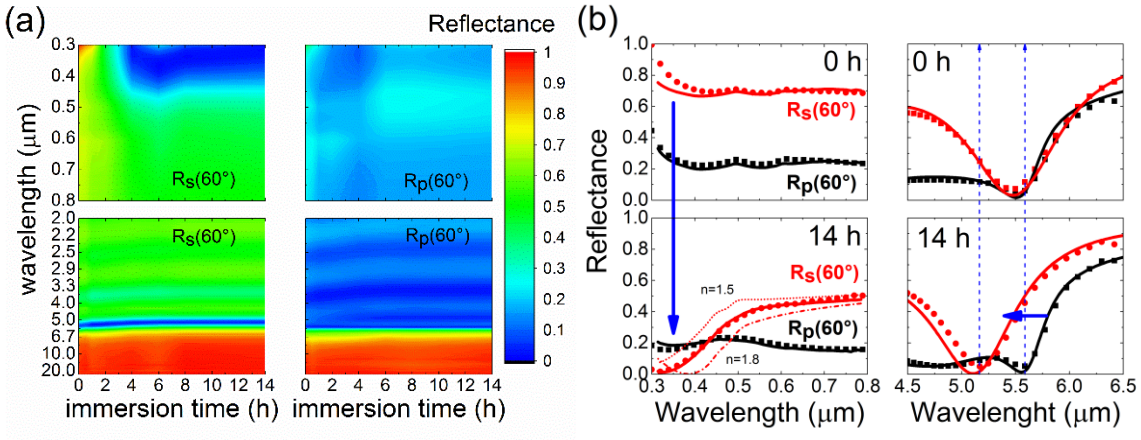

Figure 4: (a) Reflectance measurements in the visible and infrared spectral ranges for s- (left hand-side) and p-polarised (right hand-side) incident light with incidence angle of 60 degree. (b) Experimental data (points) and fitting curves (solid lines) for GaSb / InAsSb compound structure before (0 h) and after immersion to water (14 h). The dashed-dotted lines are fitting curves with different fitting values for the oxides refractive index n to illustrate an error interval for the best fit parameter.

The spectral regions where the reflectance was most affected by the immersion in water are shown in Figure 4(b). The experimental data points were fitted by solid lines calculated by the transfer-matrix method [52]. We find a good agreement between the measurement and the fitting curves. As the transfer-matrix method requires geometrical and optical material properties to calculate the reflectance of a layer structure, we rely on tabulated values for GaSb and InAs in the visible range of light. We found that reported n,k-values for GaSb are suitable to model the material in the visible range (fit range from 300-800 nm), but in the infrared range (fit range from 2-20 µm) we rely on an analytical expression to describe the refractive index of GaSb [3]. The highly Si-doped InAsSb can be described by tabulated n,k-data of InAs in the visible spectral range. In the IR-range the semiconductor behaves like a metal due to the high doping. Therefore InAsSb can be described by the Drude-model in the IR-range [48]. Here, we report the value of $\omega_p = 1.05 \cdot 10^{15}$ rad/s, $\gamma_p = 1.3 \cdot 10^{13}$ rad/s and $\varepsilon_\infty = 10.4$ as input parameter to the Drude equation to describe the IR-permittivity of InAsSb. The good agreement between the measured (black data points) and simulated reflectance (black line) in the visible range shows that the layer structure before immersion can be described by tabulated n,k-data (GaSb) for the 50 nm thick GaSb toplayer and tabulated n,k-data (InAs) for the InAsSb layer. This suggests that good material quality was obtained by MBE-growth. Fitting the measured reflectance in the infrared range allows to determine ω_p and γ_p describing the metallic behavior of InAsSb. The absorption losses in the residual doped-GaSb wafer are accounted in the model by assuming the substrate to be semi-infinite. After 14 h of immersion the top-layer has become transparent to visible light as expected from Raman measurements. The obtained fit (red line) of the data (red data points) was obtained by assigning a value of n = 1.6 to the 50 nm thick oxide layer. In Figure 4(b) the simulated curves for fit parameters of n = 1.5 and 1.8 (dashed dotted lines) are added to demonstrate an error range for the fit value. The strongest sensitivity on the fit parameter is observed in the range from 300 to 400 nm. This can be explained in terms of an anti-reflective-coating effect of the oxide toplayer where the $\lambda/4$ –criterion, $\lambda_0/(4 \cdot n)$, is fulfilled for an index of refraction of $n = 1.6 \pm 0.1$ (for incident light λ_0 of 300 nm and for a 50 nm toplayer). We conclude this part by comparing the found fit value for the gallium oxide formed from GaSb in water with similar materials in the spectral range from 0.3 to 20 µm. The found value of $n = 1.6 \pm 0.1$ is slightly lower than the reported values for anodically grown GaSb oxides ($n \approx 2.0$), but in good agreement with the refractive index value reported for Ga_2O_3 (n=1.68) [44]. The higher refractive index of anodically formed GaSb

oxide is probably due to the presences of antimony oxides, which are depleted by a slow corrosion process (several hours) when GaSb is immersed in water.

6. Discussion of results and proposed band structure

The measurements performed to characterize the oxidation of crystalline GaSb upon immersion in deionized water reveal that the oxidized layer is transparent to light in the visible, is mainly composed by gallium and oxygen, is non-conductive and has a comparable thickness as the reagent layer. Good fitting of its optical properties can be achieved by assuming a constant refractive index of $n = 1.6 \pm 0.1$ from 0.3 µm to 20 µm. We suggest water splitting, oxygen incorporation and antimony-dissolution as reaction mechanisms, which transforms GaSb into a gallium oxide when immersed in deionized water. The end product of this reaction is a Ga-rich wide-band gap oxide.

While the band structure of crystalline $InAs_{1-x}Sb_x$ / GaSb is well established, there exists a multitude of gallium and antimony oxides each with different crystal properties and band structures. A priori, we do not know if the material transition in deionized water leads to a known crystalline Ga-oxide configuration. Nevertheless, we can compare material properties derived from our study with those in the literature for Ga_2O_3 [44]. We find good agreement in terms of band gap (here > 4.0 eV) and refractive index (here $n = 1.6 \pm 0.1$, compared to 1.68-1.74 for literature values). As the band offset between GaSb and InAsSb prevents the free-carriers in the highly Si-doped InAsSb ($\sim 5x10^{19}$ cm^{-3}) to diffuse into the non-doped GaSb, a similar band offset seems plausible for the Ga-oxide. Assuming that the electron affinity X of the oxide formed in deionized water is close to the electron affinity of GaSb and β-Ga_2O_3 we summarize our findings in an energy band diagram. In Figure 5(a), the out-of-equilibrium band alignment shows the GaSb/InAsSb before immersion in water. The changes in band-gap due to the depletion of antimony and the incorporation of oxygen are shown in Figure 5(b). The proposed energy band diagram explains the Raman measurement results, i.e. the appearance of InAsSb phonon modes upon immersion in water, and it explains the insulating behavior of the Ga-oxide toplayer.

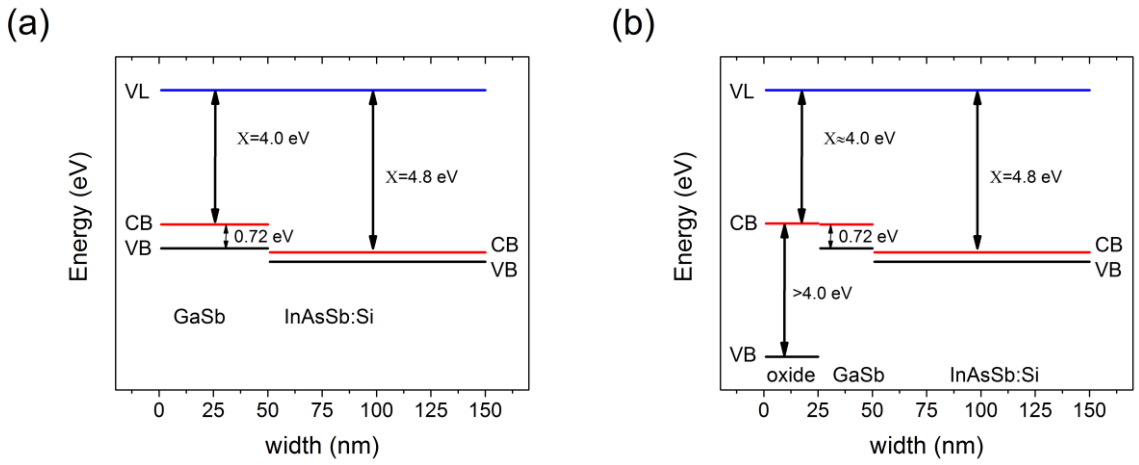

Figure 5: (a) Band alignment for GaSb / InAsSb heterostructure before immersion in water. (b) Proposed band structure to explain the transparency and the insulating behaviour of 50 nm thick toplayer upon GaSb oxidation in water.

7. Conclusion

We have shown that crystalline GaSb undergoes a material transition in water. The investigated model compound system of a 50 nm thick GaSb layer on a 1000 nm thick highly Si-doped InAsSb layer was grown by molecular beam epitaxy. The InAsSb:Si serves as a chemical stop layer and a high conductive mid-IR plasmonic layer. We find that 50 nm of GaSb transforms within 14 h to Sb-depleted Ga oxide. Already after 4 h of reaction time, the low-band gap material GaSb, opaque to visible light, transforms to a transparent material. Subsequently, the remaining antimony oxide continues to dissolve into solution such that the final product is a gallium oxide. The good conductivity of the

highly Si-doped InAsSb and the absence of conduction states through the gallium oxide was demonstrated by tunneling atomic force microscopy. Measuring the reflectivity of the compound layer structure from 0.3 to 20 µm and fitting the data by the transfer-matrix method allowed to determine a refractive index value of 1.6 ± 0.1 for the oxide formed in water. The investigated model system demonstrates that corrosion, i.e. antimony depletion and oxygen incorporation, transforms the narrow band gap material GaSb into a gallium oxide transparent in the range from 0.3 to 20 µm. This study shows that the III-V semiconductor mid-IR plasmonic material platform based on GaSb can be combined with a gallium oxide surface.

Funding

French Investment for the Future program (EquipEx EXTRA, ANR 11-EQPX-0016); French ANR (SUPREME-B, ANR-14-CE26-0015); European Union's Horizon 2020 research and innovation programme (Marie Sklodowska-Curie grant agreement No 641899); Occitanie region.

Acknowledgements

J.-M. Peiris and J. Lyonnet are acknowledged for technical support at the cleanroom facilities of the Université de Montpellier. G. Boissier, J.-M. Aniel and G. Narcy are acknowledged for technical support. Frederic Pichot is acknowledged for support and advices concerning the energy-dispersive X-ray spectroscopy measurements. Michel Ramonda is acknowledged for support and advices regarding the tunneling atomic force microscopy measurements. Jean-Baptiste Rodriguez and Anthony Phimphachanh are acknowledged for discussion of the oxidation reaction mechanism.

References

1. B. R. Bennett, R. Magno, J. B. Boos, W. Kruppa, and M. G. Ancona, "Antimonide-based compound semiconductors for electronic devices: A review," Solid-State Electron. **49**, 1875–1895 (2005).
2. A. Krier, ed., *Mid-Infrared Semiconductor Optoelectronics*, Springer Series in Optical Sciences No. 118 (Springer, 2006).
3. S. Roux, P. Barritault, O. Lartigue, L. Cerutti, E. Tournié, B. Gérard, and A. Grisard, "Mid-infrared characterization of refractive indices and propagation losses in GaSb/$Al_xGa_{1-x}AsSb$ waveguides," Appl. Phys. Lett. **107**, 171901 (2015).
4. S. Roux, L. Cerutti, E. Tournie, B. Gérard, G. Patriarche, A. Grisard, and E. Lallier, "Low-loss orientation-patterned GaSb waveguides for mid-infrared parametric conversion," Opt. Mater. Express **7**, 3011 (2017).
5. L. M. Fraas, J. E. Avery, J. Martin, V. S. Sundaram, G. Girard, V. T. Dinh, T. M. Davenport, J. W. Yerkes, and M. J. O'neil, "Over 35-percent efficient GaAs/GaSb tandem solar cells," IEEE Trans. Electron Devices **37**, 443–449 (1990).
6. V. M. Andreev, S. V. Sorokina, N. K. Timoshina, V. P. Khvostikov, and M. Z. Shvarts, "Solar cells based on gallium antimonide," Semiconductors **43**, 668–671 (2009).
7. M. P. Lumb, S. Mack, K. J. Schmieder, M. González, M. F. Bennett, D. Scheiman, M. Meitl, B. Fisher, S. Burroughs, K.-T. Lee, J. A. Rogers, and R. J. Walters, "GaSb-Based Solar Cells for Full Solar Spectrum Energy Harvesting," Adv. Energy Mater. **7**, 1700345 (2017).
8. V. N'Tsame Guilengui, L. Cerutti, J.-B. Rodriguez, E. Tournié, and T. Taliercio, "Localized surface plasmon resonances in highly doped semiconductors nanostructures," Appl. Phys. Lett. **101**, 161113 (2012).
9. T. Taliercio, V. Ntsame Guilengui, L. Cerutti, J.-B. Rodriguez, and E. Tournié, "GaSb-based all-semiconductor mid-IR plasmonics," in M. Razeghi, ed. (2013), p. 863120.
10. F. B. Barho, F. Gonzalez-Posada, M.-J. Milla-Rodrigo, M. Bomers, L. Cerutti, and T. Taliercio, "All-semiconductor plasmonic gratings for biosensing applications in the mid-infrared spectral range," Opt. Express **24**, 16175 (2016).

11. M. Bomers, F. Barho, M. J. Milla-Rodrigo, L. Cerutti, R. Arinero, F. G.-P. Flores, E. Tournié, and T. Taliercio, "Pedestal formation of all-semiconductor gratings through GaSb oxidation for mid-IR plasmonics," J. Phys. Appl. Phys. **51**, 015104 (2018).
12. M. Rei Vilar, J. El Beghdadi, F. Debontridder, R. Artzi, R. Naaman, A. M. Ferraria, and A. M. Botelho do Rego, "Characterization of wet-etched GaAs (100) surfaces," Surf. Interface Anal. **37**, 673–682 (2005).
13. Y. Zhao, R. L. Frost, J. Yang, and W. N. Martens, "Size and Morphology Control of Gallium Oxide Hydroxide GaO(OH), Nano- to Micro-Sized Particles by Soft-Chemistry Route without Surfactant," J. Phys. Chem. C **112**, 3568–3579 (2008).
14. L. Li, W. Wei, and M. Behrens, "Synthesis and characterization of α-, β-, and γ-Ga_2O_3 prepared from aqueous solutions by controlled precipitation," Solid State Sci. **14**, 971–981 (2012).
15. S. J. Pearton, J. Yang, P. H. Cary, F. Ren, J. Kim, M. J. Tadjer, and M. A. Mastro, "A review of Ga_2O_3 materials, processing, and devices," Appl. Phys. Rev. **5**, 011301 (2018).
16. D. Gogova, G. Wagner, M. Baldini, M. Schmidbauer, K. Irmscher, R. Schewski, Z. Galazka, M. Albrecht, and R. Fornari, "Structural properties of Si-doped β-Ga_2O_3 layers grown by MOVPE," J. Cryst. Growth **401**, 665–669 (2014).
17. G. P. Schwartz, "Analysis of native oxide films and oxide-substrate reactions on III-V semiconductors using thermochemical phase diagrams," Thin Solid Films **103**, 3–16 (1983).
18. C. W. Wilmsen, ed., *Physics and Chemistry of III-V Compound Semiconductor Interfaces* (Springer US, 1985).
19. Y. Mizokawa, O. Komoda, and S. Miyase, "Long-time air oxidation and oxide-substrate reactions on GaSb, GaAs and GaP at room temperature studied by X-ray photoelectron spectroscopy," Thin Solid Films **156**, 127–143 (1988).
20. C. L. Lin, Y. K. Su, T. S. Se, and W. L. Li, "Variety transformation of compound at GaSb surface under sulfur passivation," Jpn. J. Appl. Phys. **37**, L1543 (1998).
21. M. V. Lebedev, E. V. Kunitsyna, W. Calvet, T. Mayer, and W. Jaegermann, "Sulfur Passivation of GaSb(100) Surfaces: Comparison of Aqueous and Alcoholic Sulfide Solutions Using Synchrotron Radiation Photoemission Spectroscopy," J. Phys. Chem. C **117**, 15996–16004 (2013).
22. D. Tao, Y. Cheng, J. Liu, J. Su, T. Liu, F. Yang, F. Wang, K. Cao, Z. Dong, and Y. Zhao, "Improved surface and electrical properties of passivated GaSb with less alkaline sulfide solution," Mater. Sci. Semicond. Process. **40**, 685–689 (2015).
23. N. C. Henry, A. Brown, D. B. Knorr, N. Baril, E. Nallon, J. L. Lenhart, M. Tidrow, and S. Bandara, "Surface conductivity of InAs/GaSb superlattice infrared detectors treated with thiolated self assembled monolayers," Appl. Phys. Lett. **108**, 011606 (2016).
24. R. Stine, E. H. Aifer, L. J. Whitman, and D. Y. Petrovykh, "Passivation of GaSb and InAs by pH-activated thioacetamide," Appl. Surf. Sci. **255**, 7121–7125 (2009).
25. J. Mäkelä, M. Tuominen, M. Yasir, M. Kuzmin, J. Dahl, M. P. J. Punkkinen, P. Laukkanen, K. Kokko, and R. M. Wallace, "Oxidation of GaSb(100) and its control studied by scanning tunneling microscopy and spectroscopy," Appl. Phys. Lett. **107**, 061601 (2015).
26. M. V. Lebedev, T. V. Lvova, and I. V. Sedova, "Coordination of the chemical and electronic processes in GaSb(100) surface modification with aqueous sodium sulfide solution," J. Mater. Chem. C **6**, 5760–5768 (2018).
27. M. Bomers, A. Mezy, L. Cerutti, F. Barho, F. Gonzalez-Posada Flores, E. Tournié, and T. Taliercio, "Phosphonate monolayers on InAsSb and GaSb surfaces for mid-IR plasmonics," Appl. Surf. Sci. **451**, 241–249 (2018).
28. O. Dier, C. Lin, M. Grau, and M.-C. Amann, "Selective and non-selective wet-chemical etchants for GaSb-based materials," Semicond. Sci. Technol. **19**, 1250–1253 (2004).
29. E. Papis-Polakowska, "Surface treatment of GaSb and related materials for the processing of mid-infrared semiconductor devices," Electron Technol. Internet J. **37**, 1–34 (2005).
30. D. Seo, J. Na, S. Lee, and S. Lim, "Behavior of a GaSb (100) Surface in the Presence of H_2O_2 in Wet-Etching Solutions," J. Phys. Chem. C **119**, 24774–24780 (2015).
31. D. Seo, J. Na, S. Lee, and S. Lim, "Behavior of GaSb (100) and InSb (100) surfaces in the presence of H2O2 in acidic and basic cleaning solutions," Appl. Surf. Sci. **399**, 523–534 (2017).
32. S. A. Jewett, J. A. Yoder, and A. Ivanisevic, "Surface modifications on InAs decrease indium and arsenic leaching under physiological conditions," Appl. Surf. Sci. **261**, 842–850 (2012).

33. K. Tsunoda, Y. Matsukura, R. Suzuki, and M. Aoki, "Thermal instability of GaSb surface oxide," in B. F. Andresen, G. F. Fulop, C. M. Hanson, J. L. Miller, and P. R. Norton, eds. (2016), p. 98190S.
34. O. V. Sulima, A. W. Bett, and J. Wagner, "Anodic Oxidation of GaSb in Acid-Glycol-Water Electrolytes," J. Electrochem. Soc. **147**, 1910–1914 (2000).
35. V. M. Bermudez, "First-principles study of the interaction of H_2O with the GaSb (001) surface," J. Appl. Phys. **113**, 184906 (2013).
36. A. L. Pitman, M. Pourbaix, and N. de Zoubov, "Potential-pH Diagram of the Antimony-Water System," J. Electrochem. Soc. **104**, 594 (1957).
37. L. A. Wills, X. Qu, I.-Y. Chang, T. J. L. Mustard, D. A. Keszler, K. A. Persson, and P. H.-Y. Cheong, "Group additivity-Pourbaix diagrams advocate thermodynamically stable nanoscale clusters in aqueous environments," Nat. Commun. **8**, 15852 (2017).
38. Y. Mao and A. Krier, "Energy-Band offsets and electroluminescence in n-InAs 1-x Sb 1-x/N-GaSb heterojunctions grown by liquid phase epitaxy," J. Electron. Mater. **23**, 503–507 (1994).
39. K. J. Cheetham, P. J. Carrington, A. Krier, I. I. Patel, and F. L. Martin, "Raman spectroscopy of pentanary GaInAsSbP narrow gap alloys lattice matched to InAs and GaSb," Semicond. Sci. Technol. **27**, 015004 (2012).
40. M. Muñoz, K. Wei, F. H. Pollak, J. L. Freeouf, and G. W. Charache, "Spectral ellipsometry of GaSb: Experiment and modeling," Phys. Rev. B **60**, 8105–8110 (1999).
41. D. E. Aspnes, B. Schwartz, A. A. Studna, L. Derick, and L. A. Koszi, "Optical properties of anodically grown native oxides on some Ga-V compounds from 1.5 to 6.0 eV," J. Appl. Phys. **48**, 3510 (1977).
42. S. Zollner, "Model dielectric functions for native oxides on compound semiconductors," Appl. Phys. Lett. **63**, 2523–2524 (1993).
43. S. Gowtham, M. Deshpande, A. Costales, and R. Pandey, "Structural, Energetic, Electronic, Bonding, and Vibrational Properties of Ga_3O, Ga_3O_2 , Ga_3O_3 , Ga_2O_3 , and GaO_3 Clusters," J. Phys. Chem. B **109**, 14836–14844 (2005).
44. H. He, R. Orlando, M. A. Blanco, R. Pandey, E. Amzallag, I. Baraille, and M. Rérat, "First-principles study of the structural, electronic, and optical properties of Ga_2O_3 in its monoclinic and hexagonal phases," Phys. Rev. B **74**, (2006).
45. M. Mohamed, K. Irmscher, C. Janowitz, Z. Galazka, R. Manzke, and R. Fornari, "Schottky barrier height of Au on the transparent semiconducting oxide β-Ga_2O_3," Appl. Phys. Lett. **101**, 132106 (2012).
46. N. Tigau, V. Ciupina, and G. Prodan, "The effect of substrate temperature on the optical properties of polycrystalline Sb_2O_3 thin films," J. Cryst. Growth **277**, 529–535 (2005).
47. J. P. Allen, J. J. Carey, A. Walsh, D. O. Scanlon, and G. W. Watson, "Electronic Structures of Antimony Oxides," J. Phys. Chem. C **117**, 14759–14769 (2013).
48. T. Taliercio, V. N. Guilengui, L. Cerutti, E. Tournié, and J.-J. Greffet, "Brewster “mode” in highly doped semiconductor layers: an all-optical technique to monitor doping concentration," Opt. Express **22**, 24294 (2014).
49. M. Wojdyr, "*Fityk* : a general-purpose peak fitting program," J. Appl. Crystallogr. **43**, 1126–1128 (2010).
50. D. M. Di Paola, A. V. Velichko, M. Bomers, N. Balakrishnan, O. Makarovsky, M. Capizzi, L. Cerutti, A. N. Baranov, M. Kesaria, A. Krier, T. Taliercio, and A. Patanè, "Optical Detection and Spatial Modulation of Mid-Infrared Surface Plasmon Polaritons in a Highly Doped Semiconductor," Adv. Opt. Mater. **6**, 1700492 (2018).
51. E. D. Palik and J. K. Furdyna, "Infrared and microwave magnetoplasma effects in semiconductors," Rep. Prog. Phys. **33**, 1193–1322 (1970).
52. M. Born and E. Wolf, *Principles of Optics* (Pergamon Press, 1970).